Ferromagnetic coupled μ-phenoxo-μ-carboxylato heterodinuclear complexes based on the Cr(salen) moiety: structural and magnetic characterization†

Pablo Alborés,* Johanna Seeman and Eva Rentschler*

Received 14th April 2009, Accepted 16th June 2009
First published as an Advance Article on the web 27th July 2009
DOI: 10.1039/b907328k

The synthesis, crystal structure, and magneto-chemical characterization of two new unprecedented μ-phenoxo-μ-carboxylato heterodinuclear complexes based on the Cr(salen) moiety (salen = *N*,*N*′-bis(salicylidene)ethylenediamine), $[M^{II}(O_2C(CH_3)_3)(OH_2)_2(\mu\text{-}O_2C(CH_3)_3)(\mu\text{-salen})Cr^{III}\text{-}(O_2C(CH_3)_3)]$, M = Ni (**2**), Co(**3**) are reported. The dinuclear complexes were obtained starting from the mononuclear *trans*-$[Cr(salen)(CN)_2]PPh_4$ (**1**), whose crystal structure is also reported. They show a *trans* arrangement of the Cr(salen) unit, bridging through the phenolate O atoms to a second metal center. An additional μ_2-O_2-carboxylato bridge and a further monodentating carboxylate ligand complete the roughly octahedral Cr(III) coordination sphere. The highly distorted octahedral M(II) coordination environment is completed by two coordinated water molecules and an additional monodentating carboxylate. Variable-temperature solid-state DC magnetization studies were carried out in the 2.0–300 K range. Ferromagnetic isotropic pairwise exchange parameters were found with values of $J = 4.1$ cm^{-1} (**2**) and $J = 2.1$ cm^{-1} (**3**). Additionally, for complex **3**, a ZFS parameter, D, was employed to properly fit the experimental data. Magnetization (M) *vs.* field (H) and temperature (T) data further support the presence of this anisotropic component and confirm ground states $S = 5/2$ and $S = 3$ for **2** and **3**, respectively. Broken symmetry DFT calculations properly reproduce the experimental J values supporting the ferromagnetic exchange interaction experimentally observed. No out of phase susceptibility signal was observed in 0 DC magnetic field for both complexes. However, in the case of complex **3** a non-zero χ'' is observed when a small external field is applied below 3 K, suggesting slow relaxation of the magnetization which at 0 DC field is suppressed, probably due to efficient tunnelling relaxation pathways. The low symmetry of the Co(II) site in complex **3** may lead to the presence of transversal anisotropic components which could be responsible for the enhanced tunnelling pathway.

Introduction

Existence of ferromagnetic interactions between metal centers, which provide high S values for the ground state, and easy axis anisotropy (negative D value) of the spin ground state are the main requisites for the design of clusters with single molecule magnet (SMM) behavior.[1,2] Both of them are continuously pursued by chemists using different synthetic strategies. While quite a good understanding of the ions possessing local high values of anisotropy is available,[3] obtaining metallic clusters exhibiting ferromagnetic exchange interactions is still a difficult task even if some recent examples have been reported.[4] The usual approach towards rational design of ferromagnetically coupled systems relies on orthogonality of the interacting magnetic orbitals. Usually, the combination of t_{2g}–e_g single occupied d orbitals of the coupled metal pairs fits this scheme and is one of the main strategies used. However, the local symmetry at each metal center and the total cluster symmetry have a crucial role in the final observed interaction type between the metals.[2,5]

We have explored the reaction of a Cr(salen), (salen = *N*,*N*′-bis(salicylidene)ethylenediamine) based precursor with Co(II) and Ni(II) μ-carboxylato moieties, both of them containing potential local anisotropic ion sources. Namely, we prepared and structurally characterized for the first time the *trans*-$[Cr(salen)(CN)_2]^-$ anion as the tetraphenylphosphonium salt. This anion had been previously used for the design of cyano bridged complexes.[6] However in the presence of metal carboxylate sources, here in the case of Co(II) and Ni(II), it readily releases the cyanide ligands, retaining the stable Cr(salen) core, and affords O-phenolate salen bridged dinuclear products additionally bridged by carboxylate ligands. The new dinuclear complexes are ferromagnetically coupled, hence exhibiting non-diamagnetic ground states which in the case of

Institute of Inorganic and Analytical Chemistry, Johannes Gutenberg – University of Mainz, Duesbergweg, 10-14 D-55128, Mainz-, Germany. E-mail: albores@uni-mainz.de, rentschl@uni-mainz.de; Fax: +49 6131/39-23922

† Electronic supplementary information (ESI) available: Crystallographic characterization of complex **1**, discussion, Crystallographic information files (CIF), selected distances and angles for complex **1** (Table S1), *ORTEP* plot of complex **1** (Fig. S1 and S2), *ORTEP* plots of complexes **1**–**3** showing the H-interactions (Fig. S3), error contour plot of correlated $D_{Co} - J$ parameters of complex **3** (Fig. S4), error contour plots of correlated $g_s - D_s$ parameters of complexes **2** and **3** (Fig. S5 and S6), plot of reduced magnetization ($M/N\beta$) *vs.* H/T for a non-restrained sample of complex **3** (Fig. S7), plot of $\chi'T$ and χ'' *vs.* T for complex **3** at different driving AC frequencies under 0 DC (Fig. S8), plot of χ'' *vs.* external DC field for complex **3**, at 1.8 K with a 1500 Hz driving AC frequency (Fig. S9), and plot of $\chi'T$ *vs.* H and χ'' *vs.* H at 1.8 K for complex **2** at different driving AC frequency (Fig. S10). CCDC reference numbers 720440–720442. For ESI and crystallographic data in CIF or other electronic format see DOI: 10.1039/b907328k

the Cr(III)–Co(II) complex, exhibits a high negative *D* parameter value. None of them show out of phase signals at 0 DC in the AC susceptibility measurements. However, complex **3** does show a non-zero χ'' susceptibility component when a small external DC field is applied below 3 K. Most probably, fast tunneling relaxation pathways are operative at 0 DC field preventing the observation of non-zero χ'' signal, typical of SMM behaviour, as a moderate thermal barrier for reversal of the magnetization is expected for complex **3**, bearing a highly anisotropic Co(II) site.

We report the synthetic procedure, structural characterization and magnetic properties study of the two new ferromagnetic coupled μ-phenoxo-μ-carboxylate heterodinuclear complexes based on the Cr(salen) moiety and containing Co(II) and Ni(II) as the second metallic site. These are the first structurally characterized ever reported examples of complexes showing a Cr(salen) unit bridging additional metallic centers through the O-phenolate atoms set.

Results and discussion

Synthetic procedures

We have prepared and structurally characterized the tetraphenylphosphonium (PPh_4^+) salt of the *trans*-$[Cr(salen)(CN)_2]^-$ anion (**1**). The synthetic procedure essentially follows the reported one for the potassium salt.[7] This new salt is a relevant precursor as it allows reaction in non-aqueous solvents. Reaction of an acetonitrile solution of **1** with dinuclear Co and Ni carboxylate precursors yielded novel neutral heterometallic Cr–Co and Cr–Ni dinuclear complexes where the different metallic sites are bridged through the phenoxo-O atoms of the salen and one pivalate ligand, $[M^{II}(O_2C(CH_3)_3)(OH_2)_2(\mu\text{-}O_2C(CH_3)_3)(\mu\text{-salen})Cr^{III}(O_2C(CH_3)_3)]$, M = Ni (**2**), Co(**3**) (Scheme 1). From the reaction batch single crystals suitable for X-ray diffraction measurements are directly collected.

Most interestingly the reaction at room temperature involves the release of the cyanide ligands coordinated to the Cr(III) center. The reaction also proceeds in the dark, hence no photochemical pathways are involved. Most probably, as previously observed in other Cr(III)-cyano complexes,[8] an acid catalyzed mechanism is operative. The protons here are provided by the weakly bounded pivalic acids of the Co_2 and Ni_2 precursors.

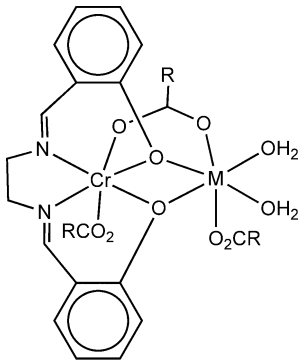

M = Ni (**2**), Co (**3**)

Scheme 1 Pictorial sketch of complexes **2** and **3**.

Structural characterization

X-Ray measurements of single crystals of **1** revealed the *trans* configuration of this dicyano anion. Surprisingly enough this is only the third structurally characterized *trans*-dicyano Cr(III) complex and the first anionic one, as the previous two examples reported correspond to cationic Cr(III) N_4-macrocycle compounds.[9] For a detailed discussion of its structure see the ESI.†

Crystal structures of complexes **2** and **3** (Fig. 1) are roughly similar. Both complexes crystallize in the orthorhombic *Pbca* space group with comparable cell parameters. Crystallographic data are shown in Table 1.

Complexes **2** and **3** show the *trans* arrangement of the Cr(salen) unit as in complex **1**, bridging through the phenolate O atoms the second metal. An additional μ-1,3-pivalato bridge and a monodentate pivalate ligand complete the roughly octahedral Cr(III) coordination sphere. The M(II) highly distorted octahedral coordination environment is completed by two coordinated water molecules and an additional monodentate pivalate ligand. Both non-bridging pivalate ligands are H-bonded to one of the coordinated water molecule (see Fig. S3†). This overall arrangement affords a Cr(III)–M(II) distance of *ca.* 3 Å. Selected distances and angles are collected in Table 2.

The $Cr–N_{salen}$ and $Cr–O_{salen}$ bond distances are almost the same as the ones observed in the precursor complex **1**, while the $Cr–O_{pivalate}$ distances are in the usual range observed in other Cr–pivalate complexes, for example Cr wheels or Cr_3–μ_3-O

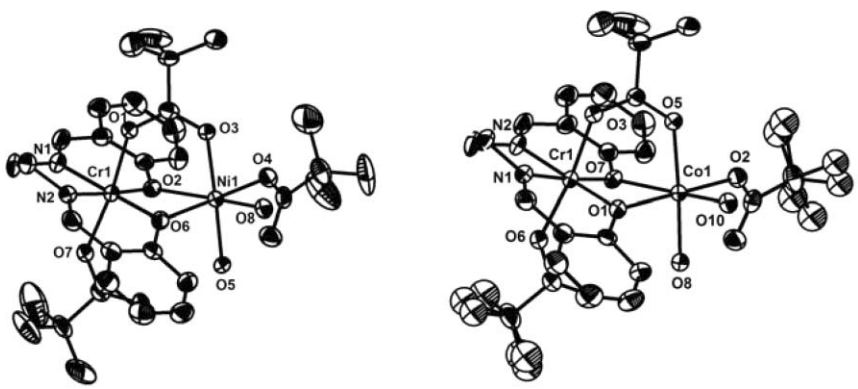

Fig. 1 *ORTEP* representation of complexes **2** (left) and **3** (right). Ellipsoid probability: 50%. Hydrogen atoms have been omitted for clarity.

Table 1 Crystal and refinement data for **1–3**

	1	**2**	**3**
Empirical formula	$C_{42}H_{34}CrN_4O_3P$	$C_{31}H_{45}CrN_2NiO_{10}$	$C_{31}H_{45}CoCrN_2O_{10}$
FW	725.70	716.40	716.62
Temperature (K)	173	173	173
Wavelength (Å)	0.71069	0.71069	0.71069
Cryst. syst.	Monoclinic	Orthorhombic	Orthorhombic
Space group	$P2_1$	*Pbca*	*Pbca*
Unit cell dimensions (Å, deg)	$a = 9.496(4)$ $b = 13.23(50)$ $c = 14.082(5)$ $\beta = 92.183(12)$	$a = 17.473(3)$ $b = 17.499(4)$ $c = 23.282(4)$	a =17.4198(3) $b = 17.6220(4)$ $c = 23.3583(6)$
Volume (Å^3)	1767.9(1)	7119.0(30)	7170.3(4)
Z	2	8	8
Density calcd. (g cm^{-3})	1.363	1.337	1.328
Abs. coeff. (mm^{-1})	0.415	0.888	0.819
$F(000)$	754	3016	3008
Cryst. size (mm^3)	$0.43 \times 0.03 \times 0.02$	$0.10 \times 0.13 \times 0.20$	$0.09 \times 0.21 \times 0.30$
θ range (deg)	1.45 to 20.31	1.75 to 28.56	1.74 to 28.46
Limiting indices	$-9 \le h \ge 9$ $-12 \le k \ge 12$ $-13 \le l \ge 13$	$-23 \le h \ge 22$ $-22 \le k \ge 22$ $-28 \le l \ge 30$	$-23 \le h \ge 23$ $-20 \le k \ge 23$ $-30 \le l \ge 30$
Reflns collected	9740	110567	123131
Ind. reflns	3413 [$R_{int} = 0.13$]	8784 [$R_{int} = 0.31$]	8897 [$R_{int} = 0.13$]
Reflns obs. [$I > 2\sigma(I)$]	2316	3207	4985
Completeness to θ (%)	99.6	96.7	98.0
Refinement method	full-matrix least-squares on F^2	full-matrix least-squares on F^2	full-matrix least-squares on F^2
Data/restraints/params	3413/1/460	8784/4/418	8897/24/410
Goodness-of-fit on F^2	0.882	0.799	0.967
Final R indices [$I > 2\sigma$(I)]	$R1 = 0.0523$, $wR2 = 0.0910$	$R1 = 0.0500$, $wR2 = 0.1907$	$R1 = 0.0579$, $wR2 = 0.1140$
R indices (all data)	$R1 = 0.0729$, $wR2 = 0.0829$	$R1 = 0.1041$, $wR2 = 0.1356$	$R1 = 0.1579$, $wR2 = 0.1818$
Largest diff. peak and hole (e Å^{-3})	0.212 and –0.215	0.783 and –0.548	1.132 and –0.734

Table 2 Selected bond lengths (Å) and bond angles (deg) of compounds **2** and **3**

	2		**3**
Ni(1)–O(5)	2.008(3)	Co(1)–O(8)	2.020(3)
Ni(1)–O(8)	2.039(3)	Co(1)–O(5)	2.064(3)
Ni(1)–O(3)	2.043(3)	Co(1)–O(10)	2.081(3)
Ni(1)–O(4)	2.056(3)	Co(1)–O(2)	2.104(3)
Ni(1)–O(6)	2.130(3)	Co(1)–O(1)	2.169(3)
Ni(1)–O(2)	2.278(3)	Co(1)–O(7)	2.319(2)
Cr(1)–O(6)	1.930(3)	Cr(1)–O(1)	1.930(3)
Cr(1)–O(2)	1.937(3)	Cr(1)–O(6)	1.946(3)
Cr(1)–O(7)	1.944(3)	Cr(1)–O(7)	1.938(3)
Cr(1)–O(1)	1.979(3)	Cr(1)–O(3)	1.991(3)
Cr(1)–N(2)	1.997(4)	Cr(1)–N(2)	2.012(3)
Cr(1)–N(1)	1.999(4)	Cr(1)–N(1)	2.013(3)
O(7)–Cr(1)–O(1)	172.39(13)	O(6)–Cr(1)–O(3)	172.29(11)
Cr(1)–O(2)–Ni(1)	91.25(12)	Cr(1)–O(1)–Co(1)	96.23(11)
Cr(1)–O(6)–Ni(1)	96.11(13)	Cr(1)–O(7)–Co(1)	91.28(10)

based systems.[10] The roughly octahedral environment of the Cr(III) site contrasts with the noticeably distorted coordination spheres around the M(II) sites. In complex **2** as well as in complex **3**, the M(II) site possesses two clearly long distances corresponding to the M–$O_{phenolate}$ bonds, one of them remarkably long, being Ni(1)–O(2), 2.278(3) Å and Co(1)–O(7), 2.319(2) Å. The remaining M(II)–O bond lengths are considerably shorter with an exception in complex **3**, where the Co–O bond length, involving the monocoordinating pivalate, is rather large, Co(1)–O(2), 2.104(3) Å. A small deviation from complete planarity for the Cr(III)–$O_{phenolate}$–M(II)–$O_{phenolate}$ core is observed in both complexes with a torsion angle of *ca.* 17°. Surprisingly, no examples are reported up to date where the Cr(salen) moiety appears bridging in a planar mode through its O-phenolate atoms, hence complexes **2** and **3** constitute the first ones. Moreover, there is only one structurally characterized example of a dinuclear complex with the planar bridging salen moiety, reported up to date, where both metal coordination spheres appear hexacoordinated, comprising a homonuclear Mn dinuclear complex.[11] However, in this example, no additional bridging ligands are present in the structure.

In both complexes, **2** and **3**, well defined H-interactions between one of the coordinated water ligands and the phenolate O atoms of the closest neighbouring molecule are clearly recognized. This affords an overall packing of well isolated pair of dimers held by H-bond interactions which leave the M(II) centers of each dimer *ca.* 4.8 Å apart (see Fig. S3†). This M(II)–M(II) inter-metallic distance is not much larger than the Cr(III)–M(II) intra-metallic one and may have some impact on the electronic structure of these dinuclear complexes.

Magnetic properties

The magnetic behaviour of the reported complexes was studied in the temperature range 2–300 K (Fig. 2) under an applied field of 0.1 T. For complex **2** the $\chi_m T$ value at 300 K is with 3.28 cm^3 K mol^{-1} slightly above the expected value for an isolated Cr(III)/Ni(II) couple ($g = 2$), 2.87 cm^3 K mol^{-1}, but it is close when a more realistic g value for Ni(II) is considered,[12] $\chi_m T$ = 3.01 cm^3 K mol^{-1} ($g_{Ni} = 2.2$). With decreasing temperature, $\chi_m T$ smoothly increases until 100 K when it suddenly rises up to a

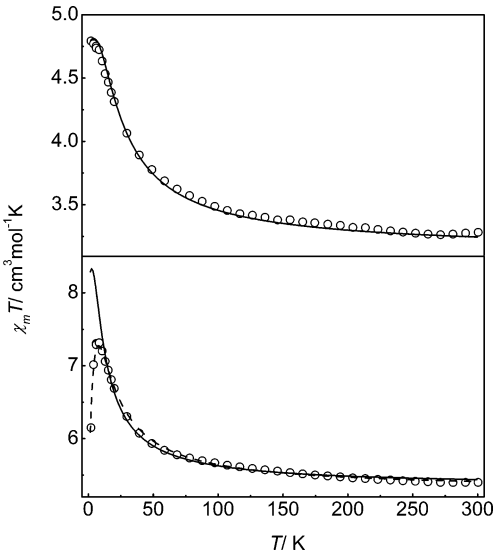

Fig. 2 $\chi_m T$ *vs.* T plots at 0.1 T of complexes **2** (top) and **3** (bottom); Full line: best fitting with Hamiltonian of eqn (2) (see text). Dashed line: best fitting with Hamiltonian of eqn (2) + ZFS contribution (eqn (3)) (see text).

maximum of 4.81 cm^3 K mol^{-1} at 2 K. This value is almost identical to the expected value for a $S = 5/2$ state ($\chi_m T = 4.82$ cm^3 K mol^{-1}, $g_{av} = 2.1$) for ferromagnetically coupled Cr(III)–Ni(II) ions.

A similar $\chi_m T$ *vs.* T plot is observed for complex **3**, with a $\chi_m T$ value at 300 K of 5.40 cm^3 K mol^{-1}, being large for isolated Cr(III)–Co(II) centers with $g_{av} = 2$, leading to 3.74 cm^3 K mol^{-1}, but in good agreement if a $g_{av} = 2.4$ is considered which gives an expected $\chi_m T$ value of 5.40 cm^3 K mol^{-1}. This big g value is related to the presence of the HS Co(II) ion which can exhibit strong anisotropic spin ground states due to first order orbital contribution.[5] The maximum in $\chi_m T$ is observed at almost the same temperature as for complex **2**, with a value of 7.31 cm^3 K mol^{-1} at 8 K. This value is somewhat below the expected value for a $S = 3$ state for ferromagnetically coupled Cr(III)–Co(II) ($\chi_m T = 8.64$ cm^3 K mol^{-1}, $g_{av} = 2.4$). At lower temperatures the $\chi_m T$ value suddenly drops probably due to the onset of zero-field splitting components. Again, as for complex **2**, $\chi_m T$ *vs.* T behaviour clearly evidences a ferromagnetic interaction between Cr(III) and Co(II) ions.

A preliminary rough estimation of the coupling strength by a Curie–Weiss treatment in the range 20–300 K gives $\theta = 7.8$ K (5.4 cm^{-1}) and $\theta = 5.8$ K (4.0 cm^{-1}) for complexes **2** and **3**, respectively. The positive value for the Weiss temperature confirms the ferromagnetic interaction.[5] We therefore attempted a full fitting of the data by obtaining the energy of the different spin states and calculating the molar susceptibility with eqn (1) for all possible field orientations:

$$\chi = \frac{1}{H}\frac{N\sum_i \left(-\partial E_i/\partial H\right)\exp\left(-E_i/kT\right)}{\sum_i \exp(-E_i/kT)} \quad (1)$$

The energy of the different spin levels is obtained through diagonalization of the suitable Hamiltonian. In this case, the Heisenberg spin Hamiltonian describing the isotropic exchange interactions between Cr(III) and M(II) ions is added to the Zeeman term:

$$\hat{H} = -2J\hat{S}_{Cr}\cdot\hat{S}_M + (g_{Cr}\beta\hat{S}_{Cr} + g_M\beta\hat{S}_M)H \quad (2)$$

The best fitting to the $\chi_m T$ *vs.* T data (Fig. 2), with the Hamiltonian of eqn (2) and fitting parameters J and an isotropic g_M factor (g_{Cr} fixed), afforded values of $g_M = 2.24 \pm 0.01$, $J = 4.1 \pm 0.2$ cm^{-1} ($R = 2.2 \times 10^{-4}$) for complex **2** and $g_M = 2.72 \pm 0.01$, $J = 1.6 \pm 0.1$ cm^{-1} ($R = 2.1 \times 10^{-4}$) for complex **3**. In both cases g_{Cr} was fixed to a value of 2.0. Changing g_{Cr} in the range 1.98–2.00, as expected for a Cr(III) ion,[12] did not modify the results within the error interval.

In case of complex **3**, $\chi_m T$ *vs.* T data was only considered up to 10 K as the inclusion of the lower temperature data set did not allow for obtaining a reasonable fit, probably reflecting the onset of strong anisotropy due to the presence of the Co(II) ion (also noticed in the large g_{Co} value). In order to take this effect into account and evaluate its impact on the data fitting we added to the Hamiltonian of eqn (2) an axial zero-field splitting (ZFS) term for the Co(II) site:

$$\hat{H}_{zfs} = D_{Co}\left(\hat{S}_{zCo}{}^2 - S_{Co}(S_{Co}+1)/3\right) \quad (3)$$

This assumes that distortion of the Co(II) ion from a perfect octahedron is big enough to remove the first-order orbital momentum by splitting the $^4T_{1g}$ ground state allowing the use of a pure spin Hamiltonian including a ZFS term.[5] In this way, over-parametrization is avoided which is implicit in the developed models that attempt to include the orbital contribution to the ground state in Co(II) complexes.[13] The best fitting to the $\chi_m T$ *vs.* T plot of complex **3** (Fig. 2), now with the Hamiltonian of eqn (2) and the additional ZFS term (eqn (3)), with fit parameters J, isotropic g_M factor (g_{Cr} fixed) and D_{Co} afforded values of $g_M = 2.70 \pm 0.01$, $J = 2.1 \pm 0.1$ cm^{-1} and $D_{Co} = 2.8 \pm 0.1$ cm^{-1} ($R = 1.8 \times 10^{-4}$). While the g_{Co} value doesn't change from the original fitting without the ZFS term, the J value is now slightly bigger and a positive D_{Co} value was obtained. The fitting improvement in the low temperature region is considerable. An error contour plot for J and D_{Co} parameters (Fig. S4†) shows a possible alternative set of parameters with negative D_{Co} (close to -12 cm^{-1}), however they afford an extremely poor quality data fitting ($R = 2.7 \times 10^{-2}$). Thus, the presence of a positive local axial ZFS parameter for the Co(II) ion is suggested from the $\chi_m T$ *vs.* T data.

The ferromagnetic isotropic exchange constant values obtained for both complexes indicate that $S = 5/2$ and $S = 3$ ground states should be found for complexes **2** and **3**, respectively, separated from the first excited state with energy differences at zero field of 20.5 cm^{-1} ($S = 3/2$) (**2**) and 12.6 cm^{-1} ($S = 2$) (**3**). To further confirm these ground state total spin values, we performed variable field (H) and temperature magnetization (M) measurements. Data were collected in the 10–70 kOe and 2–5 K ranges and are plotted in Fig. 3 as reduced magnetization. The saturation values at the highest field and lowest temperatures are 4.95 Nβ for complex **2** and 5.03 Nβ for complex **3**. In the first case, the value is quite close to the gS expected one for an $S = 5/2$ with $g = 2$ while in the second case it is clearly below the expected value for an $S = 3$ with $g = 2$. This mismatching together with the impossibility of a proper simulation of the data with an $S = 3$ Brillouin function suggests the presence of a sizeable anisotropic contribution already assumed from the $\chi_m T$ measurements. We attempted a fitting of

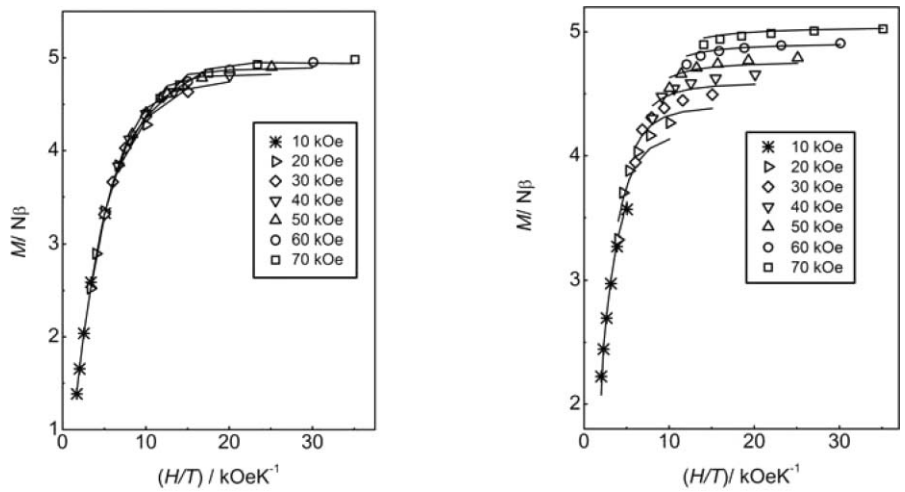

Fig. 3 Plot of reduced magnetization (M/Nβ) *vs.* H/T for complexes **2** (left) and **3** (right) in the 2–5 K range. Solid lines are the data fitting with the Hamiltonian of eqn (4) (see text).

the data (Fig. 3) by diagonalization of the spin Hamiltonian matrix considering that only the ground state is populated, incorporating axial anisotropy and Zeeman terms, and employing a full powder average. The corresponding spin Hamiltonian is given by eqn (4).

$$\hat{H} = D_S(\hat{S}_z^2 - S(S+1)/3) + g_S\beta\hat{S}H \quad (4)$$

For complex **2** with $S = 5/2$, best fitting values obtained are $g_S = 2.019 \pm 0.004$ and $D_S = -0.61 \pm 0.06$ cm^{-1} ($R = 1.59 \times 10^{-4}$). No good fitting quality is obtained when setting $D_S = 0$, even if from the $\chi_m T$ data there is no evidence of an anisotropic component; nor when trying data simulation with the full exchange-coupled Hamiltonian of eqn (2) in order to model the possible mixing with the first excited spin state ($S = 3/2$). When the error surface over g_s and D_S parameters is explored, a clear unique and defined minimum at the best fitting parameter values is found, supporting the negative sign for the axial ZFS D_S value (see Fig. S5†). Projection techniques give the relationship between the $S = 5/2$ ground state g_S and D_S values and the local g_i and D_i parameters (the anisotropic exchange coupling component has been neglected) (eqn (5)):

$$g_{\frac{5}{2}} = \frac{3}{5}g_{Cr} + \frac{2}{5}g_{Ni}\ ;\ D_{\frac{5}{2}} = \frac{3}{10}D_{Cr} + \frac{1}{10}D_{Ni} \quad (5)$$

While g_S agree quite well with the local g values obtained from $\chi_m T$ measurements, it is clear that there is no possibility of evaluating the local D_i values. However both ions Cr(III) and Ni(II) may have positive or negative D_i values[12] which can combine to afford a positive or negative D_S value, hence no contradiction is observed.

For complex **3** with $S = 3$, best fitting values obtained are $g_S = 1.94 \pm 0.03$ and $D_S = -2.1 \pm 0.2$ cm^{-1} ($R = 4.34 \times 10^{-4}$). The error surface for both parameters (see Fig. S6†) shows an additional minimum for a positive D_S value that was not considered due to the poor fitting quality, $R = 1.75 \times 10^{-3}$ ($g_S = 2.4 \pm 0.3$, $D_S = 3 \pm 3$ cm^{-1}). Fitting attempts with a pure Brillouin function with $S = 3$ clearly failed, supporting the presence of a strong anisotropy. However, this result should be analysed carefully, as the obtained D_S value (as well as the g_S value) cannot be easily rationalized from the predicted projected single ion D_i values for two coupled $S = 3/2$ spins affording an $S = 3$ ground state (eqn (6)):

$$D_3 = \frac{1}{5}D_{Cr} + \frac{1}{5}D_{Co} + \frac{3}{10}D_{CrCo} \quad (6)$$

From the fitting of the $\chi_m T$ *vs.* T data, a positive D_{Co} value is suggested which forces a non realistic quite big negative value for D_{Cr} or eventually a big negative anisotropic exchange coupling D_{CrCo} parameter value. This apparent mismatching can be understood as the break down of the strong exchange coupling limit. In fact the estimated D_{Co} value from $\chi_m T$ data is of the same order of magnitude of the exchange coupling constant J. Under this condition the total spin S is no longer a good quantum number and eqn (6) fails.[14] Comparison of these results with the one for complex **2** clearly indicates that the big negative D_s value is originated from the presence of the anisotropic Co(II) ion. Further evidence is collected when a non-restrained sample of complex **3** is used for measuring magnetization data. A completely different M *vs.* H profile is obtained (Fig. S7†). In this case magnetization is quickly saturating in a narrow range between 5.4 and 5.6 Nβ. This can be easily rationalized in terms of field induced sample torquing with subsequent orientation along the applied field together with an easy axis type anisotropy. In fact, these data can be properly fit (Fig. S7†) assuming that all the sample has been orientated with respect to the magnetic field. The orientation seems incomplete but with an angle close to 25°. With this angle, best fitting parameters are $g_s = 1.945 \pm 0.003$ and $D_s = -3.0 \pm 0.2$ cm^{-1}, ($R = 6.77 \times 10^{-5}$) which are in good agreement with the one obtained for the restrained full powder averaged sample. It should be remarked that only a negative D_s value correctly reproduces this M *vs.* H profile.

Any attempt to fit the magnetic data of complex **3** at low temperature values with an effective $S' = 1/2$ for the Co(II) ion (where only the lowest energy Kramer doublet is considered populated) completely failed. This approach usually works properly when the local symmetry of the Co(II) ion is not far away from a perfect octahedron.[13]

In view of the high negative D_s value for the $S = 3$ ground state of complex **3**, AC susceptibility measurements in the range 1.8–3.5 K at different driving frequencies were performed to

evaluate possible SMM behaviour. No out of phase susceptibility component was observed under 0 DC external field (Fig. S8†). However, when a small field is applied (up to 4 kOe) a clear non-zero χ'' signal appears evidencing slow relaxation of the magnetization (Fig. 4). When this external field is scanned at the lowest possible temperature (1.8 k) and maximum driving frequency (1500 Hz), the out of phase component smoothly increases to reach a maximum at *ca.* 1800 Oe (Fig. S9†) and then decreases to almost completely vanishing at about 4 kOe. Thus, AC susceptibility was measured at different driving frequencies in the range 1.8–3.5 K under an 1800 Oe applied external field (Fig. 5). Frequency dependence of χ'' as well as a divergence in the $\chi'T$ plot are evident, however no peak for the out of phase signal can be observed down to 1.8 K. Nevertheless, the χ'' value is quite big, reaching almost 40% of the χ' value at 1.8 K and 1500 Hz, consistent with slow magnetic relaxation observed in SMMs.[15] In order to completely discard intermolecular effects or simple paramagnet behaviour, AC measurements were also performed

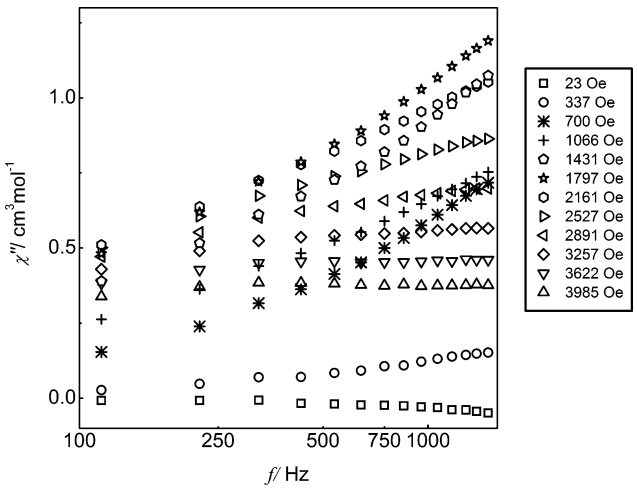

Fig. 4 Plot of χ'' *vs.* driving AC frequency (up to 1500 Hz) for complex **3** under an external DC field ranging 0–4 kOe at 1.8 K.

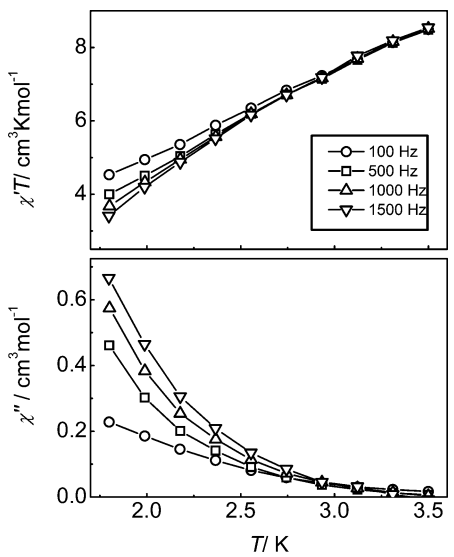

Fig. 5 Plot of $\chi'T$ (top) and χ'' (bottom) *vs.* T for complex **3** at different driving AC frequencies under an external DC field of 1800 Oe.

for the isostructural complex **2**. A strict zero out of phase signal was observed at 0 DC and also under an external applied field (Fig. S10†). These results are in agreement with the low expected magnetization reversal thermal barrier for complex **2**, $U_{eff} = |D|S^2 = 3.8$ cm^{-1} which is not enough to block magnetization down to 1.8 K. The picture is different in the case of complex **3** as a moderate value for the thermal barrier is expected, $U_{eff} = |D|S^2 = 18.9$ cm^{-1}. However, this latter expression completely relies on the strong exchange coupling limit validity which is not suitable in this case ($J \sim D$) and of course in the absence of any kind of orbital momentum contribution. Nevertheless, we still rely on it as an initial approximation to the barrier magnitude. In spite of the barrier value should be enough to block magnetization at 1.8 K, no slow relaxation process is observed in a 0 DC field, which is typical of SMM behaviour.[1] Probably, the low symmetry of the molecule allows the onset of transversal anisotropic components in the Hamiltonian, which in addition to the low S value, may lead to fast tunnelling relaxation pathways which if present, are maximized at 0 DC field due to M_s levels energy degeneracy.[1c] This phenomenon has been recently theoretically addressed for a Co_7 wheel.[16]

When a small external field is applied, the tunnelling rate can be modified by lifting the zero field degeneracy of M_S levels.[1c] Hence, the slow magnetization relaxation phenomenon observed under a small external magnetic field for complex **3** may be originated in a decrease of the tunnelling rate. In fact, the possibility of observing slow relaxation processes, otherwise absent in a 0 DC field, by application of a small external magnetic field has been recently suggested.[17]

As for the temperature dependence, no frequency maximum in the out of phase susceptibility component is observed at 1.8 K when an applied field was scanned in the range of 0–4 kOe (Fig. 4). Additionally, we couldn't observe opening in the hysteresis cycle at 1.8 K at our setup maximum field scan rate (0.004 T s^{-1}).

DFT calculations

We performed broken-symmetry (BS) DFT calculations at the X-ray geometry for complexes **2** and **3** to obtain calculated values for the isotropic exchange coupling constant *J*. Two different basis sets were used, a medium size one (*LanL2DZ*) and a big size one (*TZVP*). Previously, we have successfully employed this methodology in related systems proving this approach quite reliable.[18] The results are shown in Table 3.

The accuracy is quite remarkable and both basis sets afforded quite coincident values with the experimental ones. In both cases the right sign for the J constant value is predicted, supporting the ferromagnetic interaction between Cr(III) and M(II) ions.

Table 3 DFT calculated exchange coupling constants J and metal spin densities for complexes **2** and **3**

				Spin density Cr/M	
		J_{calc}/cm^{-1}	J_{exp}/cm^{-1}	HS	BS
2	*LanL2DZ*	5.5	4.1	2.975/1.721	2.981/−1.738
	TZVP	5.9		3.051/1.738	3.050/−1.736
3	*LanL2DZ*	0.8	2.1	2.981/2.770	2.989/−2.789
	TZVP	3.0		3.055/2.794	3.054/−2.791

Inspection of the magnetic orbitals involved, after a corresponding orbital transformation of the BS spin states, allows an insight on the origin of the observed ferromagnetic interaction. Fig. 6 shows the α–β pairs obtained for both complexes. It can be clearly noticed that all the partner magnetic orbitals are almost orthogonal to each other diminishing the antiferromagnetic pathways resulting in overall ferromagnetic coupling between Cr(III)–M(II) metallic centers. To the best of our knowledge there are no structurally characterized examples of μ-salen dinuclear complexes bearing the Cr(salen) motif in order to compare the nature and strength of the exchange interaction. The only reported example of a related system,[19] lacking structural characterization and with a poor magnetic properties study (only between 80–300 k) seems meaningless.

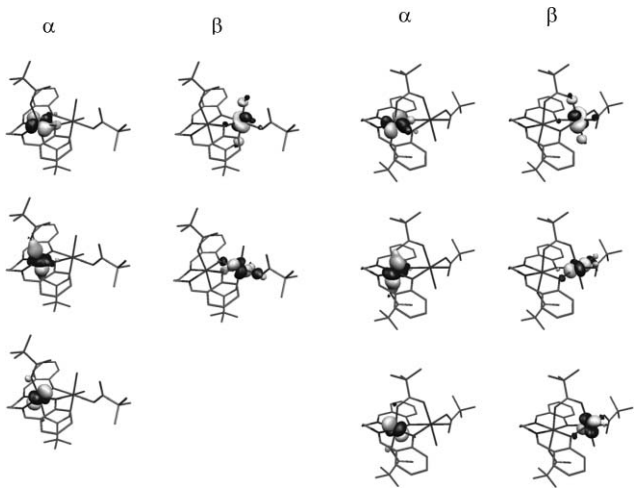

Fig. 6 α and β magnetic orbitals arising from the broken-symmetry state calculation (after a corresponding orbital transformation) of complexes **2** (left) and **3** (right). Isogrids: 0.03 a.u.

Conclusions

We have synthesized and structurally characterized two new μ-phenoxo-μ-carboxylato heterodinuclear complexes based on the Cr(salen) moiety with Co(II) and Ni(II) as the second metallic site. The *trans*-[Cr(salen)$(CN)_2$][PPh_4] precursor proved to be a suitable source of the Cr(salen) core. Both dinuclear complexes exhibit ferromagnetic interaction due to negligible overlap of the magnetic orbitals, affording ground states with $S = 3$ and $S = 5/2$ for M = Co(II) and Ni(II) respectively. DFT broken-symmetry calculations support these results. While the Cr–Ni complex spin ground state shows little anisotropy, the Cr–Co one possesses a large and negative *D* value as evidenced from magnetization measurements. No out of phase susceptibility signal was observed in a 0 DC magnetic field for complexes **2** and **3**. While in the case of complex **2** this can be understood in terms of the expected low energy for the thermal activation barrier for magnetization reversal, complex **3** is supposed to exhibit a moderate barrier. Most probably fast tunnelling processes arising from transversal Hamiltonian components are operative as the molecule possesses very low symmetry. However, a non-zero out of phase component of the susceptibility is observed when a small external field is applied. No maximum in the χ'' component is observed down to 1.8 K when the driving frequency is scanned up to 1500 Hz neither when a small DC external field is varied in the range 0–4 kOe. Unfortunately, our current setup facilities do not allow us to explore higher AC frequencies or temperatures below 1.8 K, which could provide a further insight into the magnetization dynamics of this compound.

Nevertheless, these new ferromagnetic coupled dinuclear complexes, specially the one with the Co(II) anisotropic ion, appear as promising building blocks for the design of higher nuclearity clusters exhibiting high spin ground state values and high easy axis anisotropy. Further research is currently being performed within this area.

Experimental

Material and physical measurements

[Cr(salen)$(H_2O)_2$]Cl, [Co_2(μ-OH_2)(μ-Piv)$_2$(Piv)$_2$(HPiv)$_4$] and [Ni_2(μ-OH_2)(μ-Piv)$_2$(Piv)$_2$(HPiv)$_4$] were prepared following previously reported procedures.[7,20] All other chemicals were reagent grade and used as received without further purification. Elemental analysis for C, H and N were performed on a Foss Heraeus Vario EL elemental analyzer. Infrared spectra were recorded with a Jasco FT-IR 4200 spectrophotometer with KBr pellets in the 400–4000 cm^{-1} range. Magnetic measurements were performed with a Quantum Design MPMS XL SQUID magnetometer. DC measurements were conducted from 2 to 300 K and from 0 kOe to 70 kOe. AC measurements were performed at frequencies ranging from 0.1 to 1500 Hz with an AC field amplitude of 3 Oe and applied DC field from 0 kOe to 50 kOe. Except explicitly described exceptions, all measurements were performed on restrained polycrystalline samples in order to avoid field induced reorientation of the microcrystals. Experimental magnetic data were corrected for the diamagnetism of the sample holders and of the constituent atoms (Pascal's tables).

Synthesis of the complexes

PPh_4[Cr(salen)$(CN)_2$]·$2H_2O$ (1). This complex was prepared by a modification of the reported synthesis of K[Cr(salen)$(CN)_2$]·H_2O.[7] 2.00 g (5.1 mmol) of [Cr(salen)$(H_2O)_2$]Cl were dissolved in 50 ml of 80% methanol in water. 1.70 g (26 mmol) of solid KCN were added, and the mixture was heated up to 60 °C during 1 h under stirring. After cooling down to r.t. an orange solid was obtained and was collected by filtration. After air drying 1.26 g of crude K[Cr(salen)$(CN)_2$] was obtained. It was re-dissolved in the minimum amount of water and filtered. To this clear orange solution 1.50 g (4 mmol) of solid PPh_4Cl were added. Immediately a solid appeared and the suspension was vigorously stirred for *ca.* 30 min. Then the orange solid was collected by filtration and thoroughly washed with water. After vacuum drying 1.50 g of final product were obtained. Yield: 40%. From the aqueous filtrate, single crystals suitable for X-ray were obtained after standing at r.t. for several days. Anal. Calcd. for $C_{42}H_{34}CrN_4O_2P·2H_2O$ C: 67.64, H: 5.14, N: 7.51. Found: C: 68.00, H: 4.72, N: 7.66. IR, KBr: *ν*C≡N, 2112 (vw) cm^{-1}, 2125 (vw) cm^{-1}.

[Ni^{II}($O_2C(CH_3)_3$)(OH_2)$_2$(μ-$O_2C(CH_3)_3$)(μ-salen)Cr^{III}(O_2C-$(CH_3)_3$)]·$0.5CH_3CN$ (2). 0.100 g (0.11 mmol) of [Ni_2(μ-OH_2)(μ-Piv)$_2$(Piv)$_2$(HPiv)$_4$] dissolved in 10 ml of acetonitrile and 0.070 g

(0.09 mmol) of **1** dissolved in 10 ml of acetonitrile were mixed. The resulting dark orange solution was filtered to remove some powder developed and left standing undisturbed slowly evaporating at r.t. After a few days orange crystals suitable for X-ray appeared. One of them was used for structural determination and the remaining ones collected by filtration, washed with acetonitrile and air dried. Yield: 20 mg, 30%. Anal. Calcd. for $C_{32}H_{49}CrN_2NiO_{10}\cdot 0.5CH_3CN$ C: 52.40, H: 6.56, N: 4.70 Found: C: 49.87, H: 5.96, N: 5.05.

$[Co^{II}(O_2C(CH_3)_3)(OH_2)_2(\mu\text{-}O_2C(CH_3)_3)(\mu\text{-salen})Cr^{III}(O_2C\text{-}(CH_3)_3)]$ (3). 0.100 g (0.11 mmol) of $[Co_2(\mu\text{-}OH_2)(\mu\text{-}Piv)_2(Piv)_2\text{-}(HPiv)_4]$ dissolved in 10 ml of acetonitrile and 0.070 g (0.09 mmol) of **1** dissolved in 10 ml of acetonitrile were mixed. The resulting dark red solution was filtered to remove some powder developed and left standing undisturbed slowly evaporating at r.t. After a few days red crystals suitable for X-ray appeared. One of them was used for structural determination and the remaining ones collected by filtration, washed with acetonitrile and air dried. Yield: 30 mg, 45%. Anal.Calcd. for $C_{32}H_{49}CrN_2CoO_{10}$ C: 52.46, H: 6.74, N: 3.82 Found: C: 51.67, H: 6.20, N: 4.21.

X-Ray structure determination. Crystals suitable for X-ray diffraction were obtained directly from the synthetic procedure and mounted in a glass fiber. The crystal structures were determined with a Bruker Smart APEX II CCD area-detector diffractometer using graphite-monochromated Mo-Kα radiation (λ = 0.71073 Å) at 173 K. Data was corrected for absorption with *PLATON*[21] using a multi-scan semi-empirical method. The structures were solved by direct methods with *SHELXS-97*[22] and refined by full-matrix least-squares on F^2 with anisotropic displacement parameters for non-H atoms with *SHELXL-97*.[23] Hydrogen atoms were added geometrically and refined as riding atoms with a uniform value of U_{iso} with the exception of hydrogen atoms of coordinated water molecules that were located in the difference map. Hydrogens of the non- coordinated water molecule in the complex **1** crystal structure were not found in the difference map and hence not included in the model. Two *tert*-butyl groups of pivalates coordinated to the Co atom in complex **3** crystal structure were disordered over two positions and refined isotropically in a 0.65:0.35 occupation factor ratio.

DFT quantum computations. Density functional theory (DFT) spin-unrestricted calculations were performed at the X-ray geometry using the *Gaussian03* package (revision *D.01*)[24] at the B3LYP level employing the *LanL2DZ* and *TZVP* basis sets. Tightly converged (10^{-8} E_h in energy) single point calculations were performed for the HS (high spin) and BS (broken symmetry) states in order to analyze the exchange coupling between the metallic centers. The HS- and BS-energies were then combined to estimate the exchange coupling parameter J involved in the widely used Heisenberg–Dirac–van Vleck Hamiltonian:

$$\hat{H}_{HDvV} = -J\hat{S}_A\hat{S}_B \quad (7)$$

The methodology applied here relies on the broken symmetry formalism, originally developed by Noodleman for SCF methods, which involves a variational treatment within the restrictions of a single spin-unrestricted Slater determinant built upon using different orbitals for different spins.[25] This approach has been latterly applied within the frame of DFT.[26] We employ here the approximation described by Yamaguchi and co-workers, who relate the exchange coupling parameter to the energies and expectation values of the spin-squared operator for the HS ($M_S = S_A + S_B$) and BS ($M_S = |S_A - S_B|$) states.[27]

$$J = -\frac{E_{HS} - E_{BS}}{\langle\hat{S}^2_{HS}\rangle - \langle\hat{S}^2_{BS}\rangle} \quad (8)$$

We also employed the BS-type spin unrestricted solutions after a corresponding orbital transformation as a means of visualizing the interacting non-orthogonal magnetic orbitals.[28] Note that these orbitals do not have a well-defined orbital energy. In the figures showing such orbitals, we therefore do not give orbital energies explicitly. Our main interest is the occupation and spin-coupling patterns.

Acknowledgements

We gratefully acknowledge the Alexander von Humboldt Foundation for granting a post-doctoral fellowship. This work was partially supported by the National Center for Supercomputing Applications under grant TG-MCA05S010.

References

1 (*a*) G. Christou, D. Gatteschi, D. N. Hendrickson and R. Sessoli, *MRS Bull.*, 2000, **25**, 66–71; (*b*) D. Gatteschi, R. Sessoli, J. Villain, *Molecular Nanomagnets*, Oxford University Press, 2006; (*c*) D. Gatteschi and R. Sessoli, *Angew. Chem., Int. Ed.*, 2003, **42**, 268–297.
2 H. Oshio and M. Nakano, *Chem.–Eur. J.*, 2005, **11**, 5178–5185.
3 R. Boca, *Coord. Chem. Rev.*, 2004, **248**, 757–815.
4 C. J. Milios, R. Inglis, A. Vinslava, R. Bagai, W. Wernsdorfer, S. Parsons, S. P. Perlepes, G. Christou and E. K. Brechin, *J. Am. Chem. Soc.*, 2007, **129**, 12505–12511; C. J. Milios, A. Prescimone, A. Mishra, S. Parsons, W. Wernsdorfer, G. Christou, S. P. Perlepes and E. K. Brechin, *Chem. Commun.*, 2007, 153–155; T. C. Stamatatos, D. Foguet-Albiol, S. C. Lee, C. C. Stoumpos, C. P. Raptopoulou, A. Terzis, W. Wernsdorfer, S. O. Hill, S. P. Perlepes and G. Christou, *J. Am. Chem. Soc.*, 2007, **129**, 9484–9499.
5 O. Kahn, *Molecular Magnetism*, VCH, New York, 1993.
6 Z. H. Ni, L. F. Zhang, C. H. Ge, A. L. Cui, H. Z. Kou and J. Z. Jiang, *Inorg. Chem. Commun.*, 2008, **11**, 94–96.
7 S. Yamada and K. Iwasaki, *Bull. Chem. Soc. Jpn.*, 1969, **42**, 1463–1463.
8 (*a*) L. Jeftic and S. W. Feldberg, *J. Phys. Chem.*, 1971, **75**, 2381–2387; (*b*) Dk Wakefiel and W. B. Schaap, *Inorg. Chem.*, 1971, **10**, 306–313.
9 (*a*) R. B. Lessard, M. J. Heeg, T. Buranda, M. W. Perkovic, C. L. Schwarz, R. D. Yang and J. F. Endicott, *Inorg. Chem.*, 1992, **31**, 3091–3103; (*b*) A. M. Hemmings, J. N. Lisgarten, R. A. Palmer and D. M. Gazi, *Acta Crystallogr., Sect. C-Cryst. Struct. Commun.*, 1990, **46**, 205–207.
10 (*a*) K. V. Pringouri, C. P. Raptopoulou, A. Escuer and T. C. Stamatatos, *Inorg. Chim. Acta*, 2007, **360**, 69–83; (*b*) F. K. Larsen, E. J. L. McInnes, H. El Mkami, G. Rajaraman, E. Rentschler, A. A. Smith, G. M. Smith, V. Boote, M. Jennings, G. A. Timco and R. E. P. Winpenny, *Angew. Chem., Int. Ed.*, 2003, **42**, 101–105; (*c*) J. van Slageren, R. Sessoli, D. Gatteschi, A. A. Smith, M. Helliwell, R. E. P. Winpenny, A. Cornia, A. L. Barra, A. G. M. Jansen, E. Rentschler and G. A. Timco, *Chem.–Eur. J.*, 2002, **8**, 277–285.
11 S. H. Gou, Q. D. Zeng, Z. Yu, M. Qian, J. J. Zhu, C. Y. Duan and X. Z. You, *Inorg. Chim. Acta*, 2000, **303**, 175–180.
12 B. N. Figgis, M. A. Hitchman, *Ligand Field Theory and its Applications*, Wiley-VCH, New York, 2000.
13 (*a*) H. Sakiyama, R. Ito, H. Kumagai, K. Inoue, M. Sakamoto, Y. Nishida and M. Yamasaki, *Eur. J. Inorg. Chem.*, 2001, 2027–2032; (*b*) A. V. Palii, B. S. Tsukerblat, E. Coronado, J. M. Clemente-Juan and J. J. Borras-Almenar, *J. Chem. Phys.*, 2003, **118**, 5566–5581; (*c*) A. V. Palii, B. S. Tsukerblat, E. Coronado, J. M. Clemente-Juan and J. J. Borras-Almenar, *Inorg. Chem.*, 2003, **42**, 2455–2458; (*d*) F. Lloret, M. Julve, J. Cano, R. Ruiz-Garcia and E. Pardo, *Inorg. Chim. Acta*, 2008, **361**, 3432–3445.

14 A. Bencini, D. Gatteschi, *EPR of Exchange Coupled Systems*. Springer-Verlag, Berlin, 1990.
15 A. K. Boudalis, M. Pissas, C. P. Raptopoulou, V. Psycharis, B. Abarca and R. Ballesteros, *Inorg. Chem.*, 2008, **47**, 10674–10681.
16 L. F. Chibotaru, L. Ungur, C. Aronica, H. Elmoll, G. Pilet and D. Luneau, *J Am. Chem. Soc.*, 2008, **130**, 12445–12455.
17 M. Moragues-Canovas, C. E. Talbot-Eeckelaers, L. Catala, F. Lloret, W. Wernsdorfer, E. K. Brechin and T. Mallah, *Inorg. Chem.*, 2006, **45**, 7038–7040.
18 (*a*) P. Albores and E. Rentschler, *Eur. J. Inorg. Chem.*, 2008, 4004–4011; (*b*) P. Albores and E. Rentschler, *Dalton Trans.*, 2009, 2609–2615; (*c*) P. Albores and E. Rentschler, *Polyhedron*, 2009, **28**, 1912–1916.
19 C. T. Brewer and G. A. Brewer, *Inorg. Chim. Acta*, 1992, **196**, 1–5.
20 (*a*) G. Aromi, A. S. Batsanov, P. Christian, M. Helliwell, A. Parkin, S. Parsons, A. A. Smith, G. A. Timco and R. E. P. Winpenny, *Chem.–Eur. J.*, 2003, **9**, 5142–5161; (*b*) G. Chaboussant, R. Basler, H. U. Gudel, S. Ochsenbein, A. Parkin, S. Parsons, G. Rajaraman, A. Sieber, A. A. Smith, G. A. Timco and R. E. P. Winpenny, *Dalton Trans.*, 2004, 2758–2766.
21 A. L. Spek, *PLATON, A Multipurpose Crystallographic Tools*Utrecht University, Utrecht, The Netherlands, 2000.
22 G. M. Sheldrick, *SHELXS-97. Program for Crystal Structure Resolution*, University of Göttingen, Göttingen, Germany, 1997.
23 G. M. Sheldrick, *SHELXL-97, Program for Crystal Structures Analysis*, University of Göttingen, Göttingen, Germany, 1997.
24 M. J. Frisch, G. W. Trucks, H. B. Schlegel, G. E. Scuseria, M. A. Robb, J. R. Cheeseman, J. A. Montgomery, Jr., T. Vreven, K. N. Kudin, J. C. Burant, J. M. Millam, S. S. Iyengar, J. Tomasi, V. Barone, B. Mennucci, M. Cossi, G. Scalmani, N. Rega, G. A. Petersson, H. Nakatsuji, M. Hada, M. Ehara, K. Toyota, R. Fukuda, J. Hasegawa, M. Ishida, T. Nakajima, Y. Honda, O. Kitao, H. Nakai, M. Klene, X. Li, J. E. Knox, H. P. Hratchian, J. B. Cross, V. Bakken, C. Adamo, J. Jaramillo, R. Gomperts, R. E. Stratmann, O. Yazyev, A. J. Austin, R. Cammi, C. Pomelli, J. Ochterski, P. Y. Ayala, K. Morokuma, G. A. Voth, P. Salvador, J. J. Dannenberg, V. G. Zakrzewski, S. Dapprich, A. D. Daniels, M. C. Strain, O. Farkas, D. K. Malick, A. D. Rabuck, K. Raghavachari, J. B. Foresman, J. V. Ortiz, Q. Cui, A. G. Baboul, S. Clifford, J. Cioslowski, B. B. Stefanov, G. Liu, A. Liashenko, P. Piskorz, I. Komaromi, R. L. Martin, D. J. Fox, T. Keith, M. A. Al-Laham, C. Y. Peng, A. Nanayakkara, M. Challacombe, P. M. W. Gill, B. G. Johnson, W. Chen, M. W. Wong, C. Gonzalez and J. A. Pople, *GAUSSIAN 03 (Revision D.1)*, Gaussian, Inc., Wallingford, CT, 2004.
25 L. Noodleman, *J. Chem. Phys.*, 1981, **74**, 5737–5743.
26 L. Noodleman and E. J. Baerends, *J. Am. Chem. Soc.*, 1984, **106**, 2316–2327.
27 K. Yamaguchi, F. Jensen, A. Dorigo and K. N. Houk, *Chem. Phys. Lett.*, 1988, **149**, 537–542.
28 F. Neese, *J. Phys. Chem. Solids*, 2004, **65**, 781–785.

